Review of materials science for studying the Fleischmann and Pons effect

V. Violante[1,*], E. Castagna[1], S. Lecci[1], F. Sarto[1], M. Sansovini[1], A. Torre [1], A. La Gatta[2], R. Duncan[3], G. Hubler[4], A. El Boher[4], O. Aziz[4], D. Pease[4], D. Knies[5] and M. McKubre[6]

[1]ENEA Research Center, via E. Fermi 45, 00044 Frascati (Rome), Italy
[2]Consorzio Veneto Ricerca-TSEM, Padova, Italy
[3]Texas Tech University, Lubbok, TX, USA
[4]University of Missouri, Columbia, MO, USA
[5]Coolescence LLC, Boulder, CO, USA
[6]SRI International, Menlo Park, CA, USA

Fleischmann and Pons effect (FPE) is the production of excess power during electrochemical loading of deuterium in palladium. This effect has the following features: (1) It is a threshold effect (loading D/Pd > 0.9). (2) It is unobserved when electrochemical loading is performed with hydrogen from light water. (3) It is unexplainable as a chemical effect. (4) It occurs only if the involved materials have specific characteristics.

The present article will review aspects concerning the occurrence of FPE related to materials science, a field considered to be a key to define the effect and a research approach has been conceived to find correlations with the material status. Metallurgy, crystallographic orientation and surface morphology all together are the necessary conditions to observe the phenomenon. In general, these features affect the deuterium adsorption/absorption in palladium cathodes. On the other hand, crystal orientation seems not to be crucial for PdRh alloy. A preliminary study, based on galvanostatic electrochemical impedance spectroscopy, has been carried out to investigate the status of the electrochemical interface during the effect. Results point in the direction of a significant change in the equivalent circuit at the electrode interface, as the electrode is active.

Keywords: Cold fusion, deuterium, electrochemical loading, materials science, palladium.

Metallurgy and deuterium concentration in palladium

THE onset of the excess power production during electrochemical loading (absorption) of palladium with deuterium – the Fleischmann and Pons effect (FPE)[1] was discovered to be a threshold effect[2,3]. The deuterium concentration considered as necessary to observe the phenomenon is about 0.9 in atomic fraction (D/Pd). However, since the loading estimate is based on a four-wire measurement of the resistance of the cathode, only the average value of the gas concentration into the sample might be inferred. In some experiments, in fact, excesses have been observed also when the average concentration was around 0.8 in atomic fraction, revealing that, on the average, the system palladium–deuterium is in the beta phase region of the phase diagram.

The role of the material status has been investigated during the last decade, highlighting that some specific features of the sample are related to the occurrence of the effect[4–7]. The metallurgy has a specific role in achieving the high deuterium concentration in metal, since control of the grain and of the grain-boundary size allows control of mass transfer as well; and this may reduce the stress field inside the material[8–11]. The stress field, which in general is created by the hydrogen dissolution into the lattice, acts on the diffusion flux according to the following equation

$$J = -D\left(\nabla C - \frac{C\bar{V}}{RT}\nabla\sigma_{\text{loc}}\right), \tag{1}$$

where J is the flux, D the diffusion coefficient, C the hydrogen concentration, $\bar{V}$ the molar volume of the solute (deuterium or hydrogen), R the gas constant, T the temperature and σ_{loc} is the local stress. Equation (1) shows that the stress field may reduce the diffusive flux down to zero despite a non-zero concentration gradient. This change of the diffusive flux equation is derived from the effect of the force field, which modifies the chemical potential of the hydrogen solubilized into the lattice.

An optimized metallurgical treatment, based on cold rolling and 1 h of annealing at 850°C has been developed in order to control the sample metallurgy to achieve a satisfactory loading above the deuterium concentration threshold of 0.9 (deuterium atomic fraction). Typically, cold rolling reduces the thickness of the raw metal from

*For correspondence. (e-mail: vittorio.violante@enea.it)

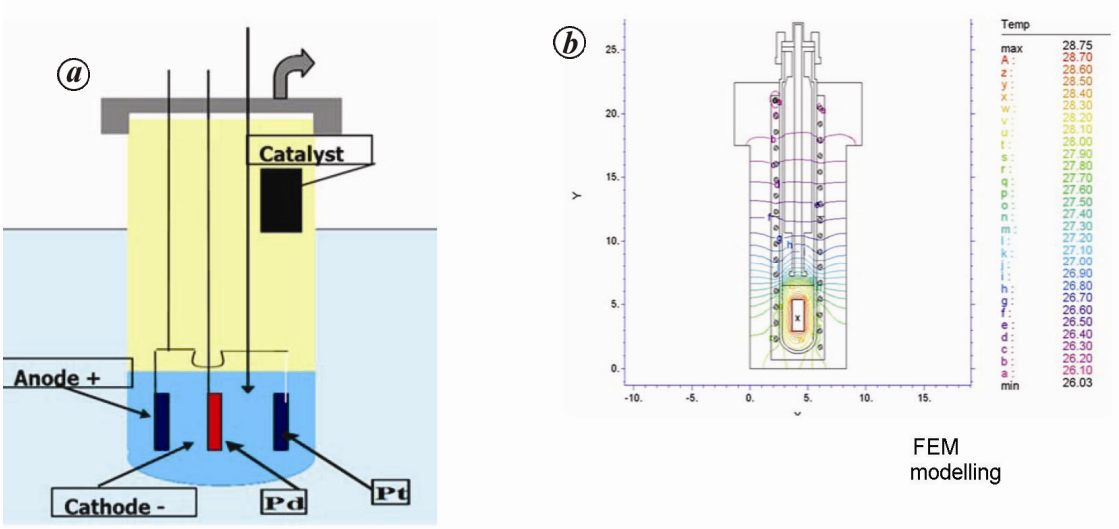

Figure 1. ***a***, Scheme of the electrochemical cell used for calorimetric measurements. ***b***, Finite element modelling of the temperature field in the calorimetric cell.

1 mm down to about 50 μm. Palladium samples characterized by a proper grain size (generally not larger than 100 μm) were realized. X-ray diffraction (XRD) is used to reveal the poly-crystalline structure of the sample. Grain orientation of Pd samples producing excess of power was mostly [100] (Miller index notation adopted). Samples produced by a raw Pd piece were identified by a lot label. Deuterium concentration in palladium, during electrochemical loading, was evaluated, as mentioned above, by means of the four-wire measurement of the electrical resistance normalized to the initial value (not loaded palladium). A confirmation of the achieved deuterium (hydrogen) concentration in our samples was done by measuring the lattice parameter elongation using XRD technique during electrolysis[12]. Both the techniques revealed that deuterium atomic fraction above 0.9 was achieved with a reproducibility close to 100%.

Palladium samples have undergone mass flow calorimetric experiments during cathodic electrochemical polarization, which is the most suitable loading technique that avoids handling of high pressure hydrogen, since an effective hydrogen (deuterium) pressure of the order of 10^5–10^6 bar is produced in this way[13].

Mass flow calorimetry

The electrochemical cell, used for calorimetric measurements, is shown in Figure 1 *a*. It is of closed type, with a catalyst capable of converting the deuterium and oxygen produced by electrolysis into heavy water. The electrodic configuration is symmetric, i.e. the cathode is located midway between two platinum foils, the electrolyte was 0.1 M LiOD and the vessel of the cell is typically pyrex. The temperature of the electrolyte was measured by a PT100 thermometer and pressure inside the cell was monitored by means of a MKS pressure gage. Figure 1 *b* shows the result of finite element modelling of temperature distribution in the cell, aimed at studying the effect of a certain thermal load and the correspondence between such a load and the response of the calorimeter.

The excess of power measurements have been mostly carried out through the mass flow calorimetry. The calorimeter scheme is shown in Figure 2. The electrochemical cell is embedded into a water jacket, which is cooled by means of a coolant pipe; the coolant is distilled water coming from a thermostatic bath (Hake type), where the temperature is controlled at the set point value with a precision of ± 0.1°C. A paraffin oil thermal filter is included in the circuit to smoothen the inlet water temperature fluctuations due to the ± 0.1°C box temperature oscillations produced by the control system. The coolant flow rate is measured and controlled by a Bronkhorst high-precision mass flow meter and controller (0.3–0.1 cm^3/s). The vessel containing the cell is insulated and placed inside a Memmert thermostatic box (± 0.1°C). The deuterium loading value is detected by means of the cathode normalized resistance measurement, performed using an HP-4284 (four-wire measurement).

Several experiments have been done using light water (LiOH 0.1 M electrolyte), obtaining a calorimeter efficiency of 97.5% (output = 0.975 × input, because of the heat losses). No production of excess power has been observed using H_2O, although a very high loading (H/Pd = 0.97) was always achieved. Temperature values are read by a Lake Shore 218 instrument and the datalogger is an Agilent hp34970a (typically the sampling time interval is 30 or 40 sec). The data acquisition system is based on LabView software. All the instruments, including the cell, have the same ground.

Such a calorimetric technique allows direct measurement of the output power, which is measured as the product of the coolant flow rate, the water specific heat and

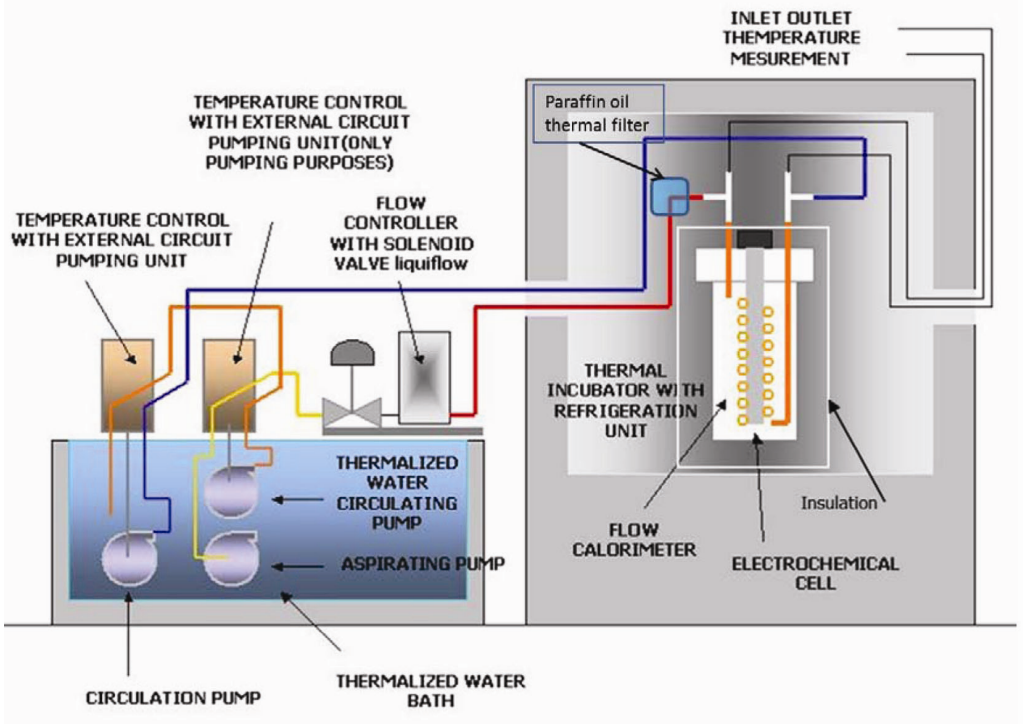

Figure 2. Scheme of the mass flow calorimetric system.

the difference between the coolant pipe outlet and inlet temperatures (both are measured by means of PT100 thermometers). The obtained value is divided by the efficiency of the calorimeter. The input power, for a galvanostatic loading condition, in DC current and closed cell, is exactly the scalar product between the cell voltage and current passing through the cell. The excess of power is given by the difference between the output power, corrected by the efficiency, and the input power. In symbols

$$P_{IN} = VI, \qquad P_{OUT} = Wc_p(T_{OUT} - T_{IN}),$$

$$P_{EX} = P_{OUT}/\text{efficiency} - P_{IN},$$

where W is the mass flow rate, c_p the water specific heat, and V and I denote the cell voltage and current respectively. The measurement uncertainty is ~5 mW at low power (<200 mW).

Possible source of errors in mass flow calorimetry can be produced by a change in the mass flow rate that would produce a little change in the efficiency of the system, or by a fast reaction between deuterium and oxygen in the cell. The first problem is overcome by an accurate coolant flow rate measurement and the second by monitoring the gas pressure into the cell, since a fast reaction would produce a pressure drop into the closed cell.

A test has been performed, using an electrochemical impedance spectrometer, in order to check how an undersampled (even not seen) oscillating voltage and current signal, nested on a DC basis, might affect the calorimetric measure. Then, a ±20 mA sine amplitude has been added above 100 mA DC, within a frequency range from 1 MHz down to 1 Hz. A sampling rate of 5 sampling per seconds has been applied. At high frequency the input power is under-sampled, according to the Nyquist theorem, and we see approximately only the average input power. As soon as the sampling rate is fast enough to produce proper sampling of the signal, we can observe the input oscillating signal; however, the output is decoupled because of the long characteristic time of the calorimeter (order of hours). Since the impedance of the electrochemical system has a real and an imaginary component, such a test takes also into account the small phase shift between current and voltage. A little change in the average input power has also been incorporated, as can be seen in Figure 3, in order to check the response of the calorimeter during the test.

This demonstrates that a fast sampling rate is not required for calorimetric purposes in this study. However, some experiments have been carried out using a data-acquisition rate up to more than a kHz.

An additional source of error could be a ground loop; this however requires detailed analysis (see Appendix 1).

Experimental evidence of excess power with mass flow calorimetry

A sample belonging to lot #64 palladium foil was treated with light water (LiOH electrolyte) using the mass flow calorimeter. Such a lot was produced from an Engelhard palladium foil 1 mm thick. A piece of the foil was rolled

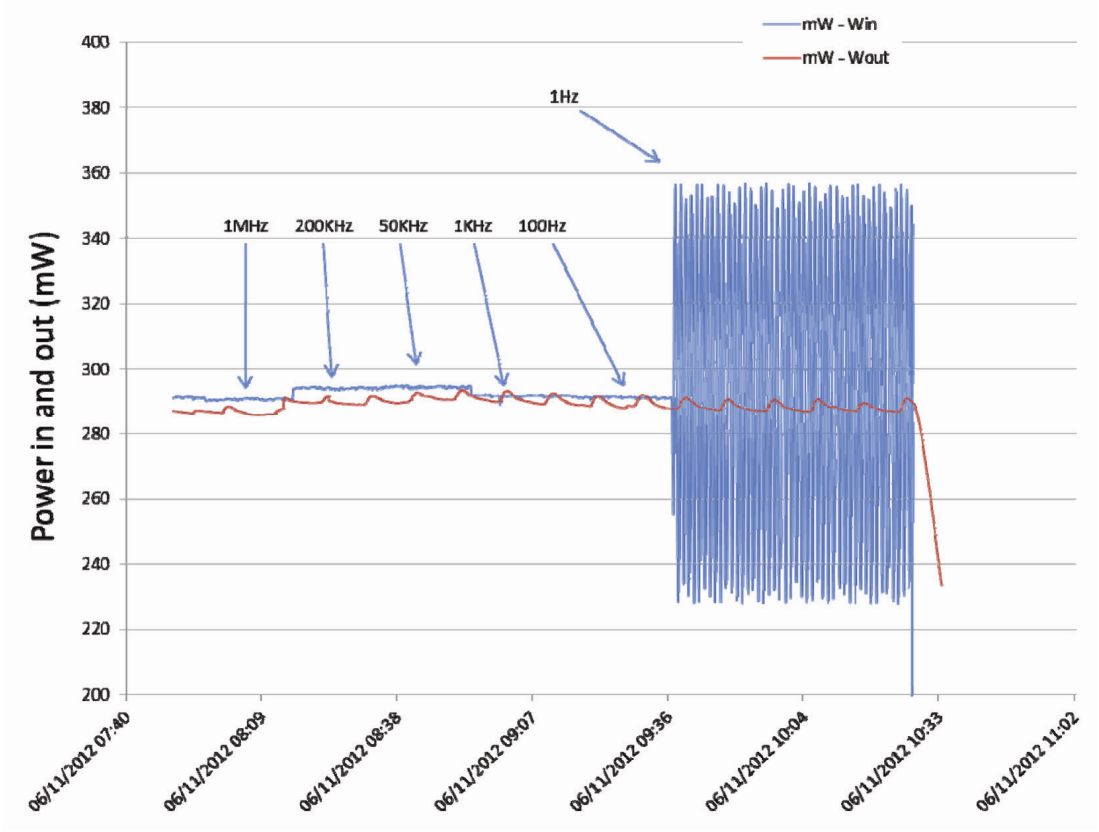

Figure 3. Effect of a ±20 mA sine amplitude nested above 100 mA DC, with a frequency range 1 MHz–1 Hz. When the sampling rate is fast enough to produce a proper sampling of the signal, we observe the input oscillating signal, however, the output is decoupled because of the long characteristic time of the calorimeter.

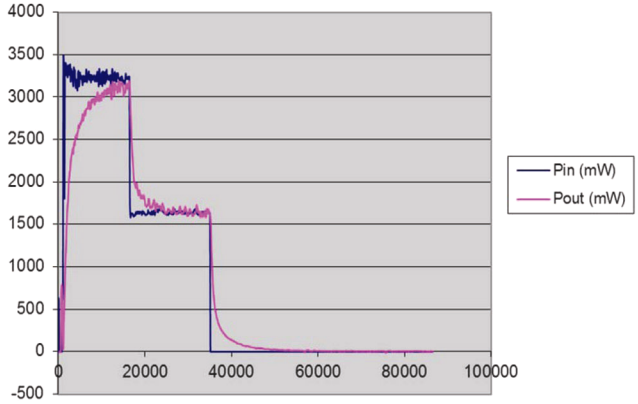

Figure 4. Calorimetric result obtained using 0.1 M LiOH electrolyte (light water). The output power perfectly overlaps the input power after the thermal transient has been overcome.

at 50 μm and then annealed at 850°C for 1 h. The sample was cleaned with acetone, ethanol and 18 M Ohm deionized water, then etched with 1 min nitric acid and 1 min aqua regia 100% (liquid solution composed of hydrochloric acid and nitric acid in 3 to 1 volume ratio) and eventually washed again in 18 M Ohm water. Figure 4 shows the calorimetric result obtained during the palladium cathode loading with hydrogen. We clearly observe that the output power perfectly overlaps the input power as soon as the thermal transient has been overcome (a similar behaviour is always observed using inactive electrodes with heavy water).

A different behaviour was observed when another sample, belonging to the same #64 lot, was treated with 0.1 M LiOD electrolyte. This sample underwent to the same cleaning and etching procedure as above described. After loading and thermal transient of the calorimeter, some heat bursts were detected. Figure 5 shows two small excess power bursts, followed by a third of larger amplitude yielded by the sample. The excess of power may occur as a burst, as in the present case, or as a signal, which remains stable for a significant time interval. In general, bursts release a higher gain in percentage, but have a short life.

Clearly, the output curve goes above the input during the bursts and the outputs curve again overlaps the input as soon as the excess power disappears. The excess of power was up to 80% of the input power. The evolution of the normalized electric resistance was consistent with an average concentration of deuterium above 0.8 in atomic fraction (D/Pd) during the excess of power. The acquired data, as we will see in the following, will help

us clear doubts concerning the considered possible sources of measurement errors.

Figures 6 and 7 show the evolution of pressure inside the cell and of the coolant flow rate respectively. We can see that the pressure behaviour is consistent with the absence of pressure drops during the excess. However, at the beginning of the experiment, we observe a pressure drop, which corresponds to the narrow burst above the noise, shown in Figure 5. This is due to the reaction between deuterium and oxygen, and hence is clearly a chemical effect. The evolution of the coolant flow rate shows that, during the excess power, its value remains perfectly equal to that initially set.

Noteworthy, two other samples belonging to the same lot gave excess power during electrochemical loading with deuterium even of larger amplitude.

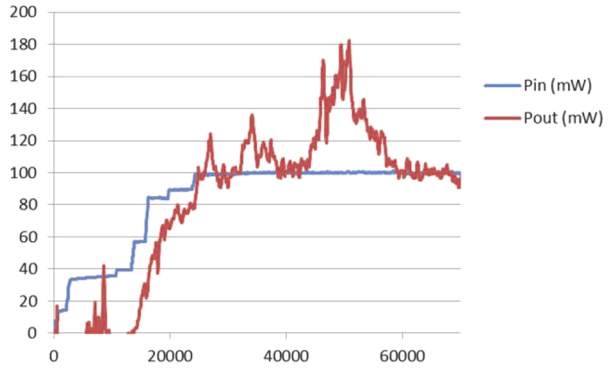

Figure 5. Excess power observed with an active palladium sample with 0.1 M LiOD. Some heat bursts are detected after the loading and the thermal transient of the calorimeter. The output curve goes above the input curve.

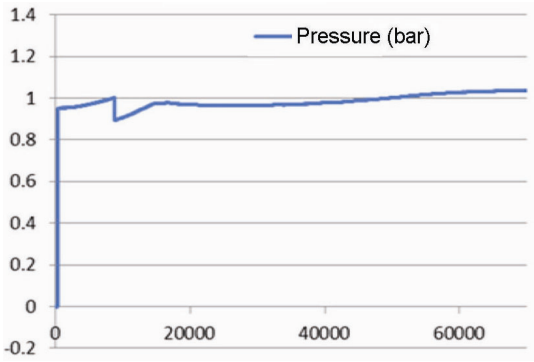

Figure 6. Evolution of gas pressure into the cell. The pressure behaviour shows the absence of pressure drops during the excess. At the beginning of the experiment, we observe a pressure drop, corresponding to the narrow burst above the noise (see Figure 5), due to the chemical reaction between deuterium and oxygen.

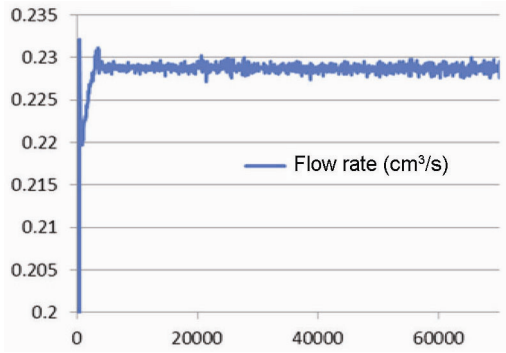

Figure 7. Evolution of the coolant flow rate. This parameter is very stable during the event.

Study of the #64 lot characteristics

Six samples belonging to lot #64 have undergone electrochemical loading (one with hydrogen, as above described, and five with deuterium). Three of the samples loaded with deuterium were active and gave excess power. All the samples underwent the same chemical cleaning and etching procedure. One of the active samples of lot #64, which gave the largest signal (average 2500%)[14], was analysed using a scanning electron microscope (SEM) before etching. Such a large amplitude signal is rarely observed, but it is well known[15].

Figure 8 *a* shows the SEM image of the sample, with grain size ranging from a few tens of microns up to about 100 μm, as revealed by a study of the grain size distribution. After running the experiment, a sample scraped from the electrode region bound inside the Teflon support, and therefore excluded from electrolysis, was examined using SEM and atomic force microscope (AFM). Such a sample, with a certain approximation, was considered as a representative after etching and of significant active status.

Figure 8 *b* shows the SEM image of the sample surface after chemical etching; a rough surface structure is seen. Figure 8 *c* shows the AFM image of a 20×20 μm^2 surface region of the sample after etching.

It was decided to characterize the surface morphology. For this, the power spectral density of the surface roughness (the squared modulus of the surface roughness Fourier transform) was considered the appropriate merit figure, since peaks at certain values of the k vector reveal the existence of structures that periodically reproduce on the surface at a distance $\lambda = 2\pi/k$. The basic idea was to try to find a correlation between the shape of the power spectral density function (PSDF), showing peaks around some k values, and the occurrence of excess power. Some other correlations between the material features and the effect have also been studied, as discussed below.

The radial PSDF of sample #64 is shown in Figure 9 (we will always consider the radial PSDF). One can observe two large peaks at $k = 1$ and $k = 2$ μm^{-1} and a smaller one around $k = 5$ μm^{-1}. The investigated region was limited to 20×20 μm^2 because of the AFM limits. Investigation of the merit figure (i.e. PSDF) at lower k values will be the target of a future investigation to be performed with a different instrumentation, for instance, a nanoscope.

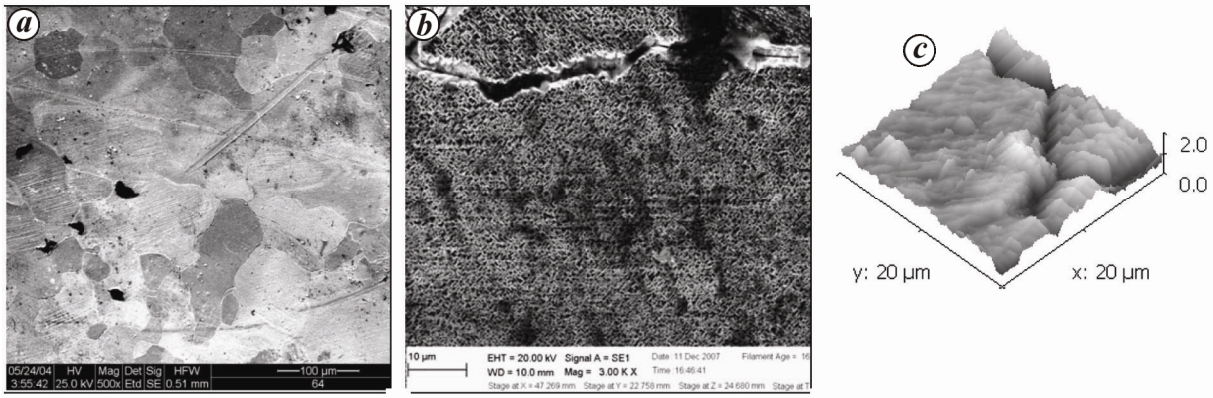

Figure 8. ***a***, ***b***, SEM image of a #64 lot sample before etching (***a***) and after etching (***b***). ***c***, AFM image of the #64 lot sample after etching.

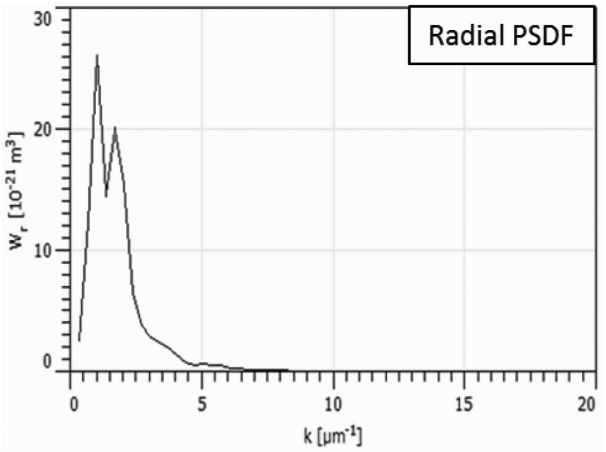

Figure 9. Power spectral density function (PSDF) of the etched sample belonging to lot #64 shown in Figure 8 *a*–*c*.

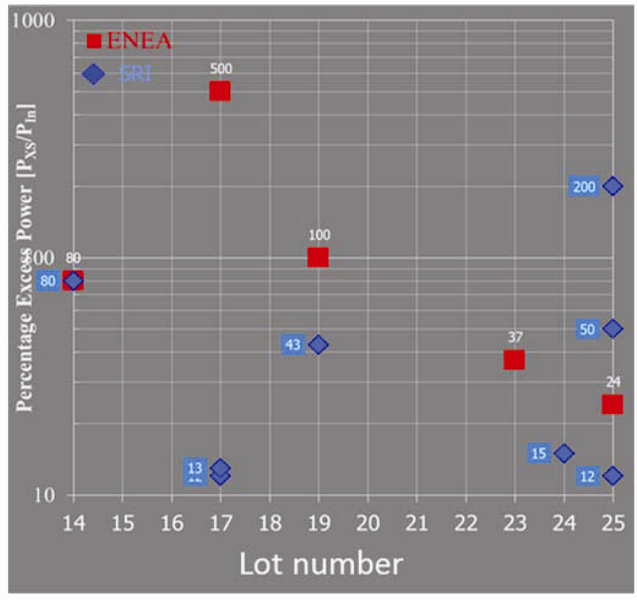

Figure 10. Synoptic of the behaviour of samples belonging to active lots experienced at ENEA (square) and SRI (rhombus). Active samples were active in both laboratories. The amplitude of the excess power was the same, or close only in some cases.

A new experimental campaign and material study

A joint work was carried out by ENEA (Italian Agency for Energy, Environment and Sustainable Development) and SRI (SRI International, CA, USA) using electrodes as described above and performing similar chemical etching. The electrodes were tested in both laboratories and most of the active area showed similar behaviour at ENEA and SRI, even if the amplitude of the signals was not always the same.

Figure 10 shows a synoptic of the behaviour of the different experienced lots in both the institutions[16].

During such a joint experimental campaign, most of the samples have been analysed and studied using SEM and AFM. Similar features were observed for the active samples as, for instance, the surface morphology identified by PSDF. Four out of six samples belonging to the lot L25 were active; Figure 11 *a* and *b* shows the AFM image and PSDF respectively, of the surface of an active sample belonging to lot L25. We again observe a rough surface with a porous structure and PSDF peaks centered near the same *k* values identified for sample #64.

The crystal orientation was also identified as a further material characteristic related to the occurrence of the effect. The additional correlation highlights that (100) orientation increases the probability of observing the effect in a PdD system (this correlation does not apply to Pd90Rh10 alloy[17]).

All the active samples giving results shown in Figure 10 have been obtained using a 'raw' Platexis palladium foil (1 mm thick), which for the sake of simplicity we will label as RAW1.

The EBSD (electron backscatter diffraction) study revealed that, after the metallurgical treatment described above (Figure 12), a [100] mostly oriented material was produced. The deuterium loading for the active samples was typically close or above 0.9 (atomic fraction).

Thus, the following material features (all needed in order to obtain an active material) can be identified: (i) Loading up to or above the threshold. (ii) Grain size up to

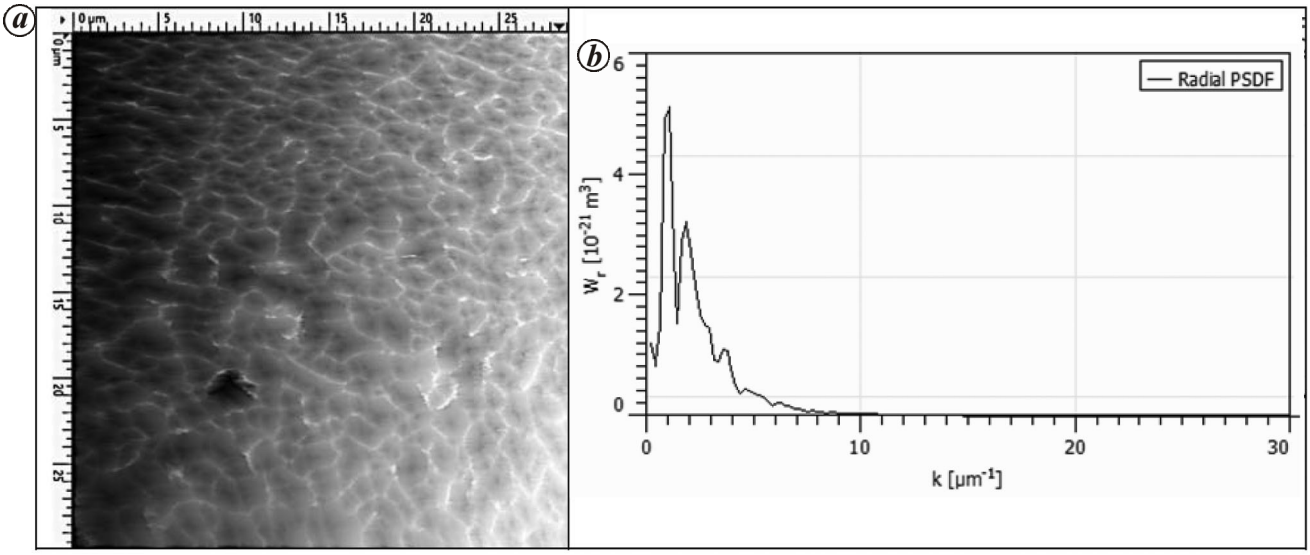

Figure 11. ***a***, AFM image (30 × 30 μm) of an active sample belonging to lot L25. Etching 2.5 min aqua regia (A.R.) 50%. ***b***, PSDF of the surface shown in (***a***). Peaks are centred near the same *k* values identified for the sample #64.

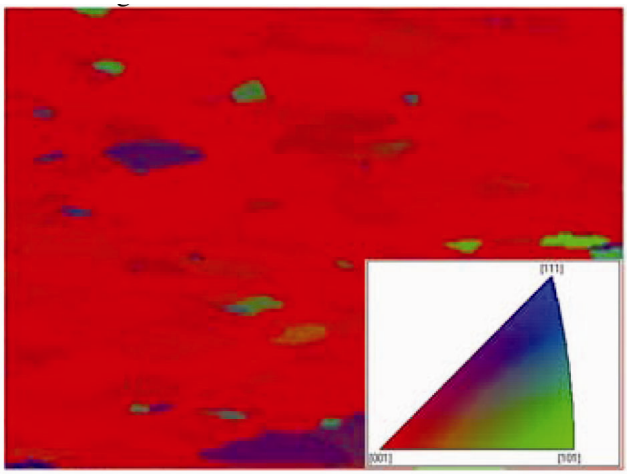

Figure 12. Metallurgical treatment performed on RAW1 palladium from Platexis yielded (100) mostly oriented samples.

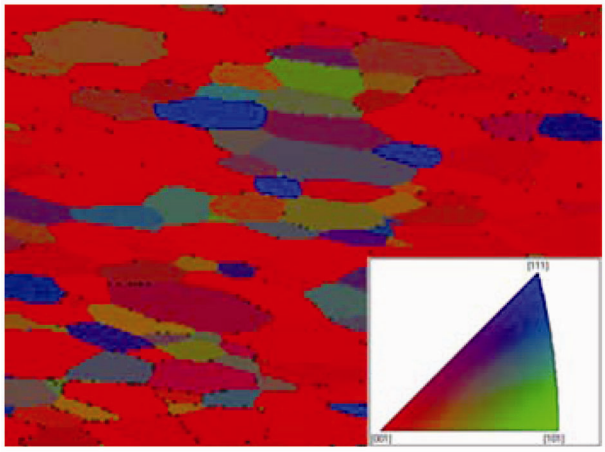

Figure 13. The same metallurgical treatment as for sample L25 performed on Platexis lot RAW2 resulted into a different crystal orientation.

about 100 μm. (iii) (100) mostly oriented material. (iv) Multi-peak shape of the PSDF.

The threshold loading is a necessary condition to observe the onset of the effect, but it is not sufficient. Indeed, all the above listed features must characterize the sample in order for it to be active. In such a case, the excess-of-power reproducibility is up to 60%.

A different raw lot from Platexis was used to continue the experimental campaign. However, the behaviour of the cathodes produced from such a lot was different; this new lot of raw material will be labelled as RAW2. First, we observed that the loading threshold was more difficult to achieve, the etching produced a different surface morphology, and the orientation of the grains was not mostly (100), as can be seen in Figure 13.

The differences in mass transfer between the two lots can be ascribed to diffusion along grain boundaries, since the two lots showed some differences in grain size distribution.

Some discussions are needed on such a specific aspect concerning diffusive mechanisms. The grain boundary diffusion (as well as the dislocation diffusion) can be important for the interaction of metals with gases for two reasons: (1) Interstitial atoms can move more rapidly along these lattice imperfections than through the undisturbed lattice. (2) They accelerate self-diffusion.

The atoms, both in small-angle and large-angle boundaries, are in many places less closely packed than in an undisturbed crystal. Then, the activation enthalpy for diffusion will often be lower at the grain boundaries

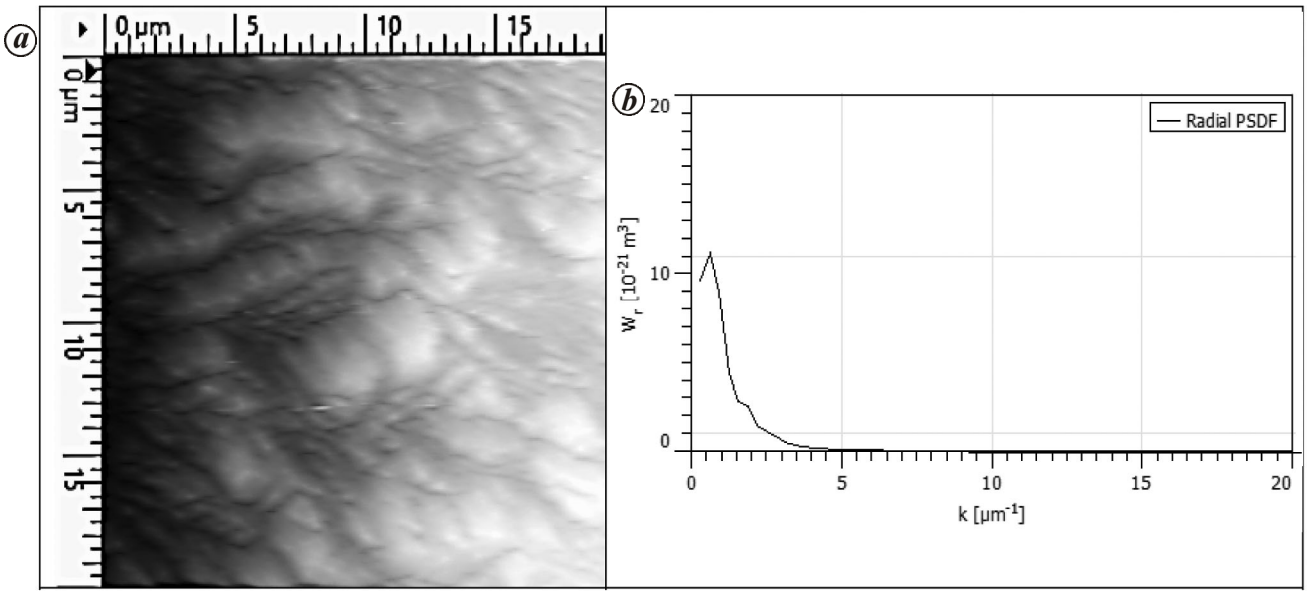

Figure 14. ***a***, AFM image of an etched (A.R. 50%) palladium sample obtained from Platexis RAW2 lot. ***b***, PSDF of the surface shown in (***a***).

than inside the grains. In any case, the fraction of the total volume available for grain boundary diffusion plays a significant role. Transport takes place mainly along the boundaries only if:

$$\frac{D(b)}{D(l)} >> \frac{\text{Average grain diameter}}{\text{Average grain boundary width}},$$

where $D(b)$ and $D(l)$ are the grain boundary and lattice diffusivities respectively. If the high-diffusivity path along a grain boundary is taken to be 1 nm wide and the grain size 100 µm, $D(b)/D(l)$ must be much greater than 10^5 in order for such a condition to be fulfilled[18]. Grain/grain-boundary diffusion equation systems have, neglecting stress effect, a closed form solution showing that the larger the product of the grain boundary size and the grain boundary diffusivity, better is the mass transfer[19].

The etching did not produce the same surface morphology. A typical surface status of the samples produced using the original Platexis lot RAW2 is shown in Figure 14 *a* and *b*. Though several experiments have been carried out using electrodes obtained from the RAW2 lot, the excess power was observed only three times and, in general, with very low amplitude and after several days of electrochemical process. Such a behaviour confirmed the importance of the material status for observing the effect. How the identified necessary features may affect the experimental conditions is described in the following.

The differences between the samples produced with RAW1 and RAW2 lots were ascribed to the contaminants; this was confirmed by the material datasheet obtained from the raw material's manufacturer. We know that contaminants may affect: (i) Grain size, which in turn affects the stress field, the mass transfer and then the loading. (ii) Crystal orientation, that acts on electrode kinetics and double layer capacitance[20]. (iii) Grain boundary, which may act on mass transfer and loading, as described above. (iv) Surface treatment[21] and morphology that act on kinetics and double-layer capacitance.

With regard to the contaminants, the main difference between RAW1 and RAW2 was in the platinum content, being 200 and 80 ppm respectively. This has led us to consider the corrosion mechanism as producing the rough surface of the active samples, which were richer in platinum. The hydrogen overvoltage on platinum is lower than on palladium; hence during the etching palladium is removed and hydrogen accumulates on platinum. This mechanism, described well in books on corrosion[22], produces a rough surface.

A designed material

On the basis of these data, a material designing work has been conceived and performed to realize a palladium cathode characterized by a proper grain size (generally not large than 100 µm), [100] mostly oriented and properly doped with platinum, in order to have a rough surface (labyrinthic or pitted) as consequence of the chemical etching. A raw material that was able to give [100] oriented samples as a result of cold rolling and annealing was selected. After producing a 50 µm thick foil, two samples were exposed to Pt sputtering on the surface, depositing a layer of 10 nm. Then, the samples were annealed in the usual manner (1 h at 850°C). Chemical etching was performed using 100% aqua regia (2 min for the first sample and 2.5 min for the second one).

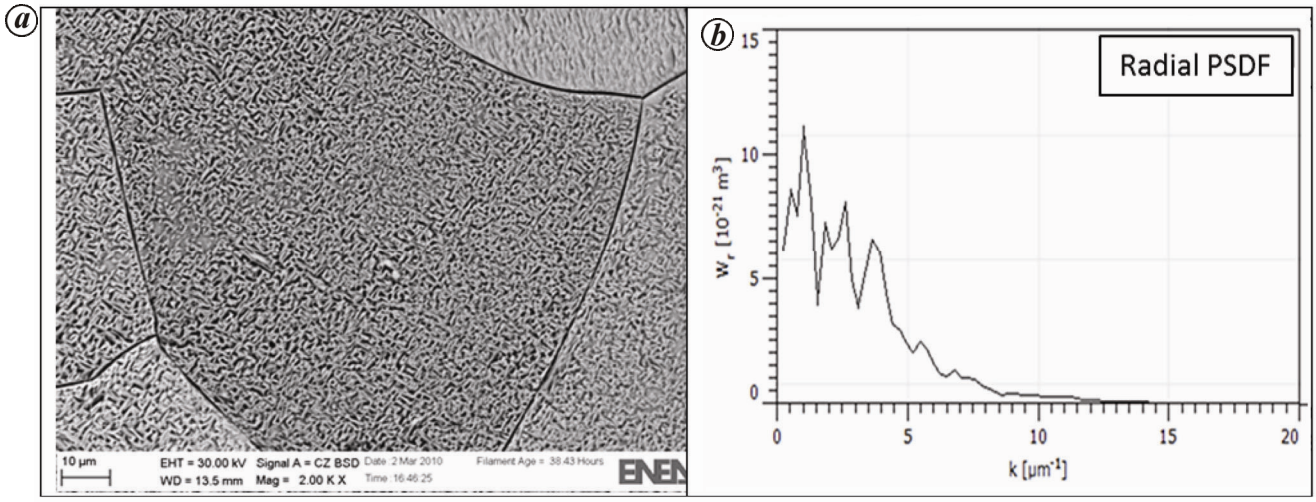

Figure 15. ***a***, SEM image of the surface of the active designed sample L66. ***b***, PSDF of the surface of the sample L66.

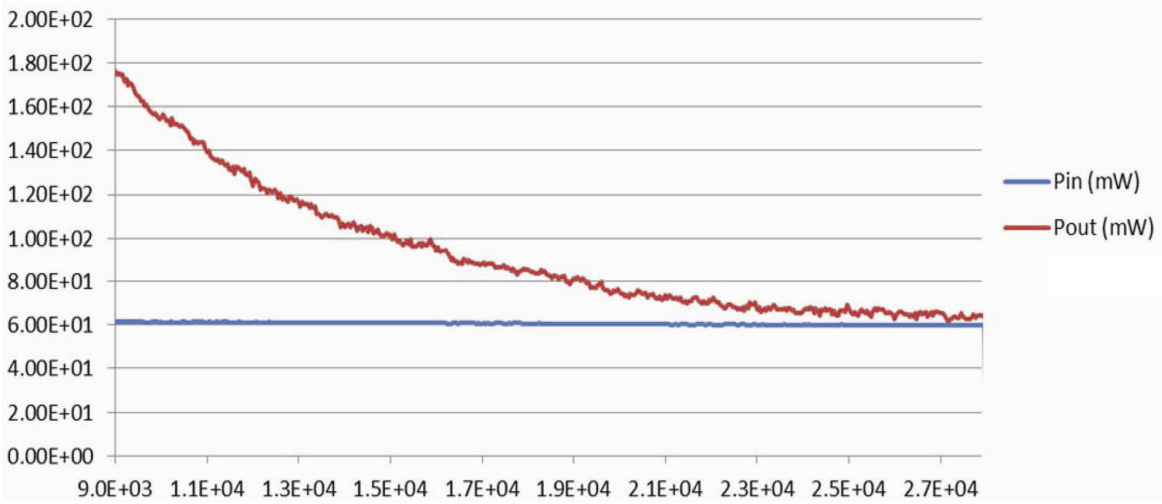

Figure 16. Details of the mass flow calorimeter display during calibration. At steady state, the output power overlaps the input power controlled at 60 mW.

The SEM analysis revealed similar status of the surface for both palladium samples, characterized by a roughness similar to that of the active samples. The PSDF for both the samples was obtained from AFM images. Figure 15 *a* shows the SEM image of the surface of one of the two samples and Figure 15 *b* the relevant PSDF (from AFM). Again, in the PSDF, we observe three significant peaks at $k = 1$, $k = 2$ and $k = 4$ µm^{-1}. Such a status was found in several points on the surface. Also, the other L66 sample showed similar surface feature.

The calorimetric test was performed for both cathodes in parallel using two identical mass flow calorimeters, which were calibrated and checked with light water electrolyte (0.1 M LiOH), using two Pd samples from a different lot. Figure 16 shows a zoomed region of the input–output power plot around 60 mW for one of the two calorimeters. Both calorimeters displayed the same behaviour during calibration. We may observe again a proper overlap of the input and output power curves at steady state at 60 mW input power. After this calibration, the two Pt-doped cathodes were compared using the calorimetric experiment.

Figure 17 shows the plot of the input and output power during the experiment performed with the sample L66. We may observe that the output curve lies above the input one. The excess is only about 20 mW, but it is detected by the calorimeter; it disappeared as soon as the input power was increased above 100 mW. The gas pressure and coolant flow rate during the effect were stable and did not affect the output power signal, as can be seen in Figure 18 *a* and *b*.

The other sample belonging to L66 lot exhibited the same behaviour in a similar mass flow calorimeter. The absence of bias was tested at the end of the

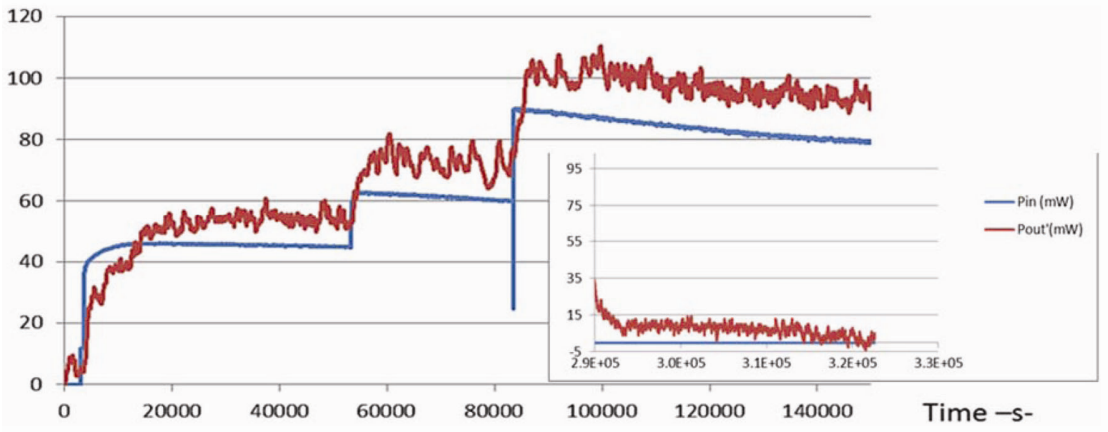

Figure 17. Input and output power during the experiment performed with the sample L66.

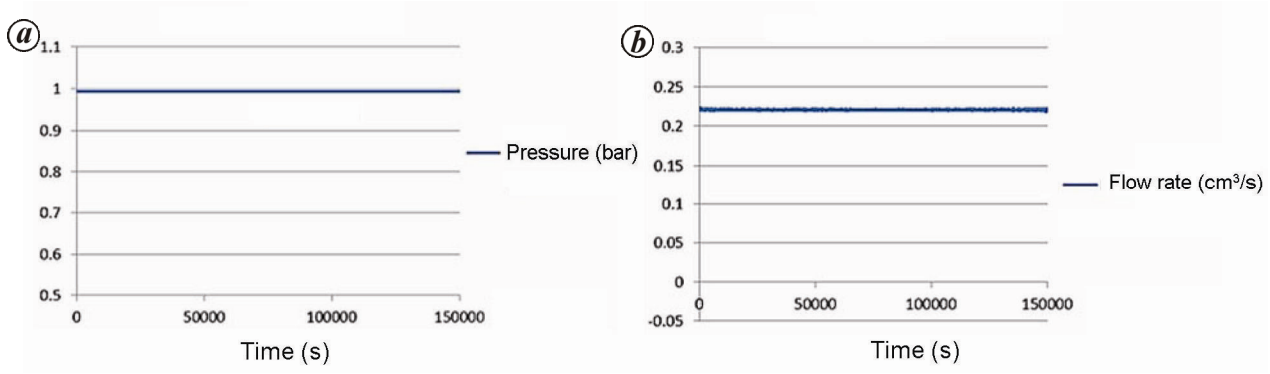

Figure 18. ***a***, Pressure inside the cell; ***b***, calorimeter coolant flow rate during the excess-power events.

experiments: the plot on the right in Figure 17 shows the overlap of the input and output power, when the input is zero, at the end of the experiment.

In both cases, during the effect, the average loading was close to 0.8 at low current (up to 25 mA). This probably was the cause of the low excess amplitude. The average deuterium atomic fraction increased up to 0.9 above 50 mA. In any case, the results confirm that there is no correlation between the surface morphology, loading rate and equilibrium concentration, since sometimes even perfectly smooth samples achieve very high loading at low current.

The relevance of the results, concerning the platinum doped samples belonging to the lot L66, does not lie in the obtained excess power (that was not extraordinary), but in the reproducibility of the effect consequent to the reproducibility of the material properties, induced by the above-described treatment.

From surface addition of platinum to Pd90Rh10 alloy and electrochemical interface characterization

Materials science research led us to the conclusion that the addition of specific elements like platinum, could increase the probability of producing the material status appropriate for the onset of the effect. Similarly, at the Naval Research Laboratory (NRL), remarkable results have been obtained with properly rhodium-doped cathodes[17]. As a consequence, the Pd90Rh10 cathodes have been prepared according to the protocol developed at the NRL[13].

Foils of palladium and rhodium were melted at 90/10 atomic ratio in an alumina crucible using a oxyacetylene torch. Then they were annealed at 900°C for 2 h and subsequently rolled to 1 mm, then annealed again at 900°C for 2 h and rolled to 50 μm. After rolling, the sample was annealed again at 900°C and etched with aqua regia. Figure 19 *a* shows the SEM image of the surface of the sample L119(20–60) after chemical etching and Figure 19 *b* shows the relevant PSDF.

Evidently, the status of the surface after the etching does not reproduce that displayed by the active electrodes. Also, the PSDF does not exhibit the typical peaks characterizing active electrodes. Despite the unsatisfactory features of the sample L119(20–60), a calorimetric study was performed using the differential calorimeter developed at NRL[23]. Such a calorimeter is a differential instrument (Figure 20). Two cells are placed inside two copper pipes nested on a common copper plate, which is equipped with a heat sink at the bottom. There is a Peltier

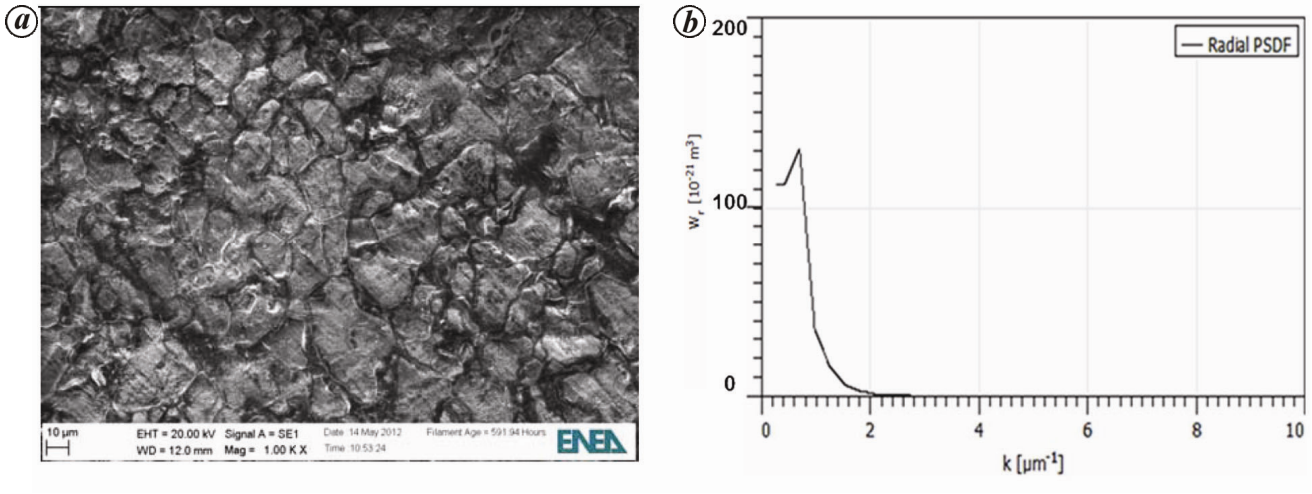

Figure 19. ***a***, SEM image of the surface of L119(20–60) $Pd_{90}Rh_{10}$ after etching (2.40 min) A.R. 50%. ***b***, PSDF of the L119(20–60)) $Pd_{90}Rh_{10}$ surface.

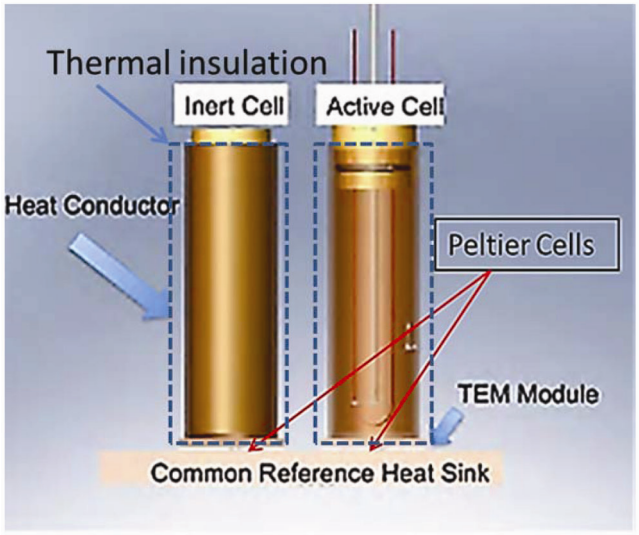

Figure 20. Naval Research Laboratory (NRL) differential calorimeter. The two cells are identical, but one acts as an electrochemical cell, while the other is a reference cell.

cell between each thermally insulated copper pipe and the copper plate.

The two cells are identical; one acts as an electrochemical cell, the other being a reference cell. The thermal flux from the active cell occurs mostly through the Peltier cell; then a calibration allows one to calculate the output power as:

$$P_{out} = a + b*\Delta V,$$

where a is the offset, b the gain, and ΔV, the electric voltage difference between the Peltier cells.

The input power is calculated as described above. Possible sources of error can be given by a crosstalk between cells or by a bias or by a ground loop (this latter case is discussed in Appendix 1). Crosstalk is identified during calibration and is produced by assembling or design. The instrument is equipped with software designed to perform additional calibration in order to check the onset of a bias when the experiment is running.

The measurement accuracy of such a calorimeter is similar to the mass flow calorimeter.

The evolution of both the input and output power is shown in Figure 21. Here, excess power spontaneously develops after ~2.90E+5 s elapsed time and remains stable for about 12 h. The electrolysis was performed using 1 M LiOD electrolyte.

From Figure 22, we observe that the evolution of the normalized resistance shows very fast loading (a few hours) at low current; a 15 mA current was enough to achieve a deuterium atomic fraction above 0.9. In general, fast loading at low current favours the onset of the effect[4].

The possible effect due to a bias of the calorimetric system was also checked by inverting the current and unloading the cathode. When the cathode was unloaded, an input power level was applied close to that existing before changing the polarity. After the thermal transient (with some adjustments of the input power at the required level), a perfect balance between the input and output power was observed; in fact, as shown in Figure 21, the relevant curves overlap. This confirms that the signal is a real effect.

The polarity was then reversed again and the PdRh cathode was reloaded at a higher current value. As soon as the cathode was reloaded (~3.55E+5 s elapsed time), the system again produced an excess power that was higher than the previous one.

Figure 23 shows the same calorimetric run after 5.30E+5 s elapsed time. Indeed, approximately at 5.82E+5 s elapsed time, with the effect still surviving, we

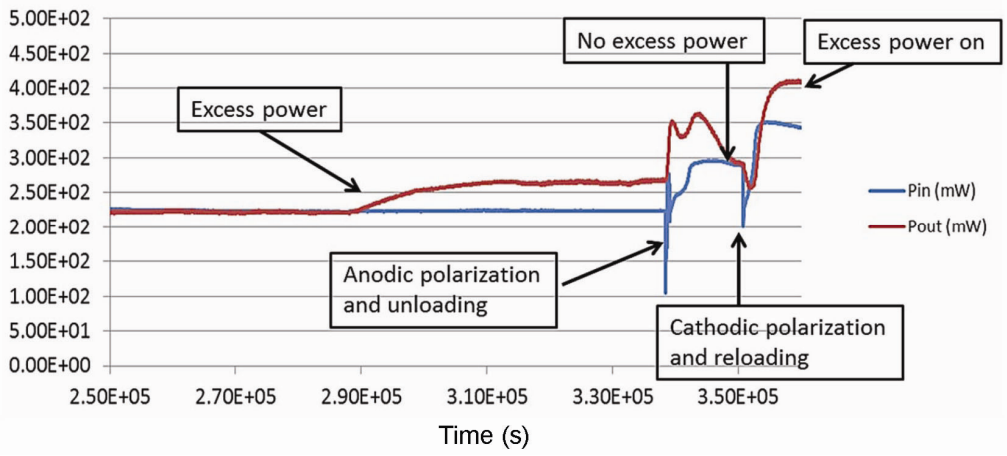

Figure 21. Excess power occurs (~2.90E+5) and is switched off by current inversion. Restoring the original cathodic polarization restarts the excess power (~3.55E+5 s).

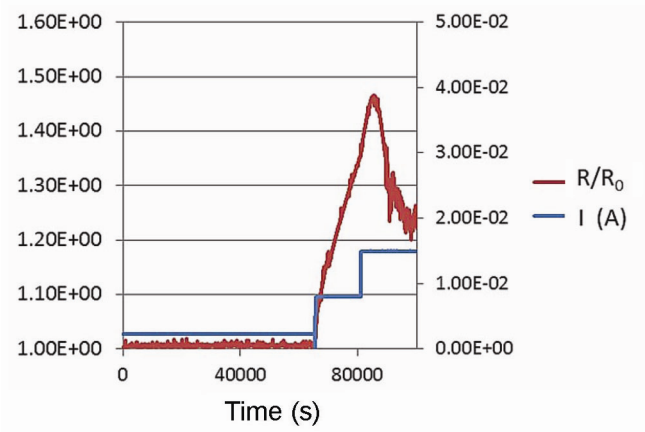

Figure 22. Evolution of the normalized resistance and current. Deuterium atomic fraction above 0.9 is achieved at low current in a few hours[29].

resolved to perform a galvanostatic electrochemical impedance spectroscopy (GEIS) measurement with the Biologic VP 200 galvanostat–potentiostat electrochemical spectrometer that was used to power and control the experiment. Electrochemical spectroscopy is a powerful technique to characterize electrode properties and the electrochemical interface. The electrochemical characterization of palladium and palladium–rhodium alloy electrodes that we performed was based on GEIS.

This experiment, which in any case should be considered as preliminary and not conclusive, was performed in order to study the possibility to extract *in situ* new information on the status of the electrochemical interface, in terms of an equivalent circuit, by comparing the typical GEIS spectrum with those obtained during the excess power. The GEIS measurements were carried out within the 400 KHz–20 Hz frequency range.

The analysis was initiated during the excess power at 100 mA DC current, but it was too noisy. Therefore, GEIS was repeated at 90 mA DC by applying 7 mA sine amplitude and some spectra were extracted. Then, the DC current was reduced to 30 mA and the excess disappeared (this confirms that there was no bias in the calorimetric system). After several hours, GEIS was repeated and the current was stopped for 1 min (no bias: the output power remains close to the input power during this current stop, because of the time constant of the calorimeter, which is of the order of thousands of seconds, as can be seen from the transient originated by the current reduction from 90 to 30 mA). Then, GEIS was repeated again. Finally, after reducing the current to zero for 1 min, the current was increased once more to 100 mA. Owing to the lower flow rate of reactants at 30 mA, the catalyst temperature was too low to induce recombination of oxygen and deuterium. The larger amount of deuterium and oxygen, produced at once by the sharp increase in current, as soon as the catalyst warmed up again, produced a fast chemical reaction inside the cell gas phase ($D_2 + O_2$). This was the chemical origin of the power burst, which can be seen in Figure 23, where all the operations above described are labelled.

The pressure drop inside the cell, shown in the top left of the figure, confirms the chemical origin of the power spike; also, it is consistent with the area of the spike in terms of energy involved. However, as can be seen in Figure 23, the current was increased and excess power survived. After a little time, it was decided to stop the experiment and remove the cathode from the cell during electrolysis, in order to maintain the status of the electrode surface as it was during the excess.

Notably, the experiment showed the possibility to control the excess, since it was switched on and off several times. In addition, we remark that the energy gain was 50 times larger than that obtainable from a possible chemical effect.

Now we first analyze the GEIS data and then extend our study to the features of the electrode in the active status. Figure 24 shows one impedance spectrum

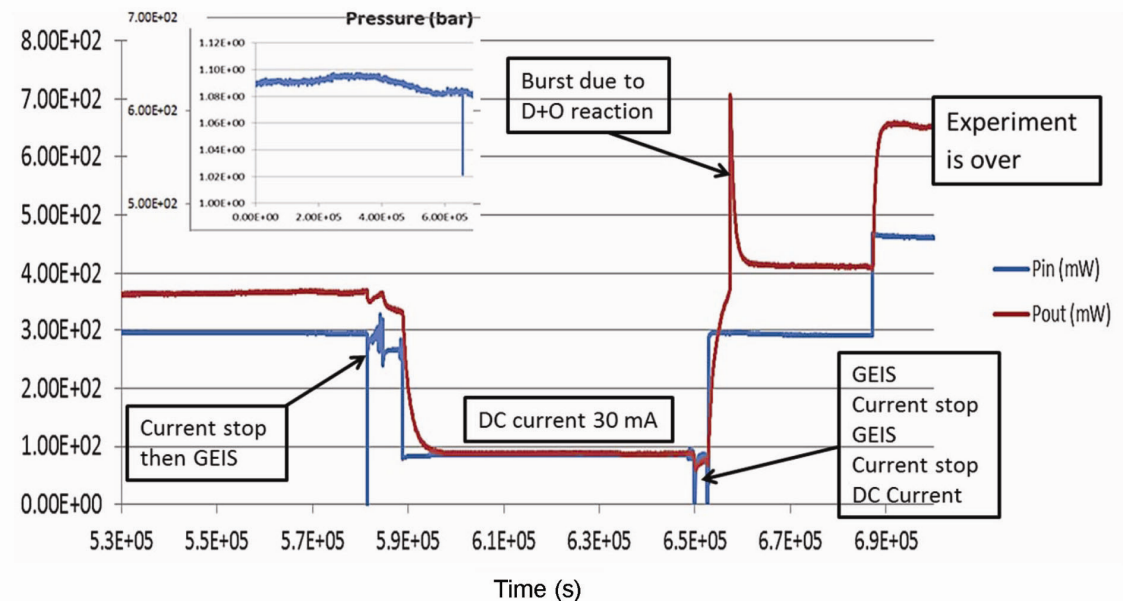

Figure 23. Input and output power during electrolysis of sample L119(20–60) Pd90Rh10. GEIS is performed during excess power at 90 mA, after switching off the excess by reducing the current first to 30 mA and then to zero. Notice that the power spike is due to a chemical effect because of a $D_2 + O_2$ reaction, as revealed by the pressure drop inside the cell (top left); the pressure drop is consistent with the area of the spike in terms of energy involved.

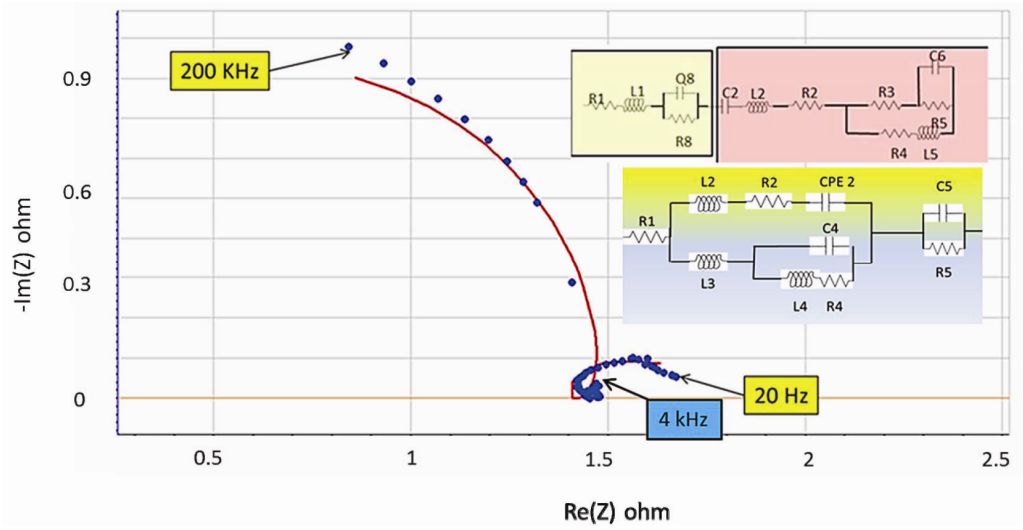

Figure 24. Impedance spectrum at 90 mA DC current and 7 mA sine amplitude, with the frequency decreasing from left to right in the plot. The most appropriate fit was obtained with two circuits, nested on the right side of the plot, that were not included into the circuit database of our electrochemical spectrometer. One of the circuits could be traced back to the one representing a partially blocked electrode.

(Nyquist plot) extracted from the data obtained at 90 mA during the excess. The circles are the experimental point and the curve represents the best fit. Such a spectrum gives a qualitative picture of the electrochemical interface when the electrode was active and producing excess power. The best fit was given by the two circuits, shown inside the figure. The one at the top right could be traced back to the electric circuit representing a partially blocked electrode[21].

As shown in Figure 25, similar spectra have been obtained at 30 mA before reducing the current to zero, when the excess power was absent (end of the plateau at 30 mA in Figure 23). This would suggest that the system was maintaining the memory of the active status.

We may observe that the current change did not affect the spectrum too much; then a semi-linear GEIS becomes acceptable. Notice that the active status was achieved again as soon as the current was increased after the last GEIS.

The reference electrode used in the experiment was a thin platinum wire inside a Teflon pipe. The end of the wire was placed close to the working electrode into the

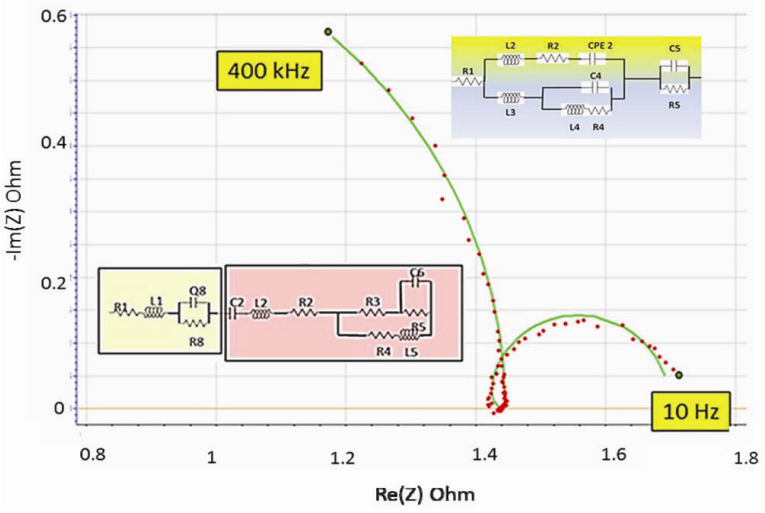

Figure 25. Impedance spectrum at 30 mA. Again, the two circuits characterized by resonant elements properly fit the experimental data.

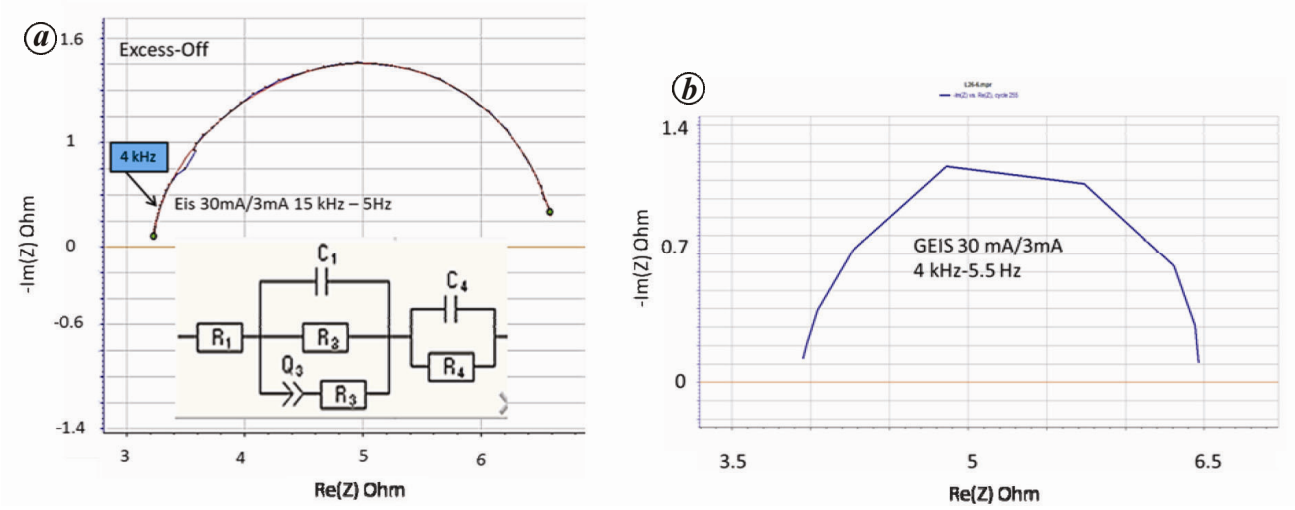

Figure 26. ***a***, Impedance spectrum at 30 mA and 3 mA sine amplitude for sample L119(20–60) after reducing the current to zero (excess off). ***b***, Typical impedance spectrum from a non-active electrode tested under the same conditions as described in (***a***).

deuterium bubbles. In principle, the reference electrode was investigating a small region of the cathode interface. Both the circuits are characterized by resonating structure and both are of interest. A blocking condition in a region is consistent with a partially blocked electrode status that, in turn, may involve high frequencies for porous structures, as reported in the literature[24]. However, the resonant frequencies of the elements, contained in the equivalent circuits shown above, are up to hundreds of kilohertz (that is the frequency limit of our impedance analysis).

GEIS was repeated at 30 mA after reducing the current to zero, the result is shown in Figure 26 *a*. In this case we observe a different shape of the Nyquist plot that is quite similar to typical impedance spectra obtained in similar conditions. Figure 26 *b* shows the impedance spectrum, given by a non-active electrode, in the same frequency range and at the same current levels as that shown in Figure 26 *a*.

The above-described results are to be considered as preliminary and further studies are necessary. However, one may conclude that the electrochemical interface substantially changes during the production of an excess of power, and that the presence of LRC components is indicative of a resonant mechanism at the interface, which is the consequence of several conditions to be achieved and controlled by the material features.

As mentioned earlier, the $Pd_{90}Rh_{10}$ cathode was removed from the cell when it was producing the excess. After drying it in the ambient, it was analysed again with SEM and AFM. Figure 27 *a* shows the SEM image of its surface, where we may observe the formation of texture which was absent before the electrolysis. The effect of texture on the shape of the PSDF can be inferred from

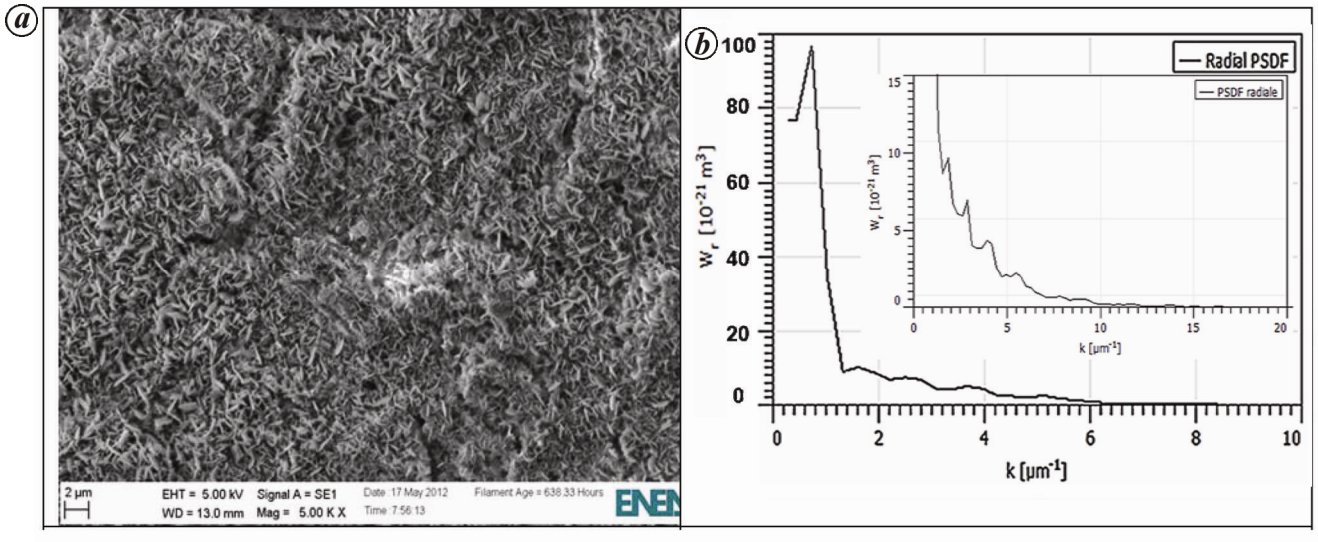

Figure 27. ***a***, SEM image of the electrode surface of L119(20–60) while producing excess power. ***b***, PSDF from AFM of sample L119(20–60) while producing excess power.

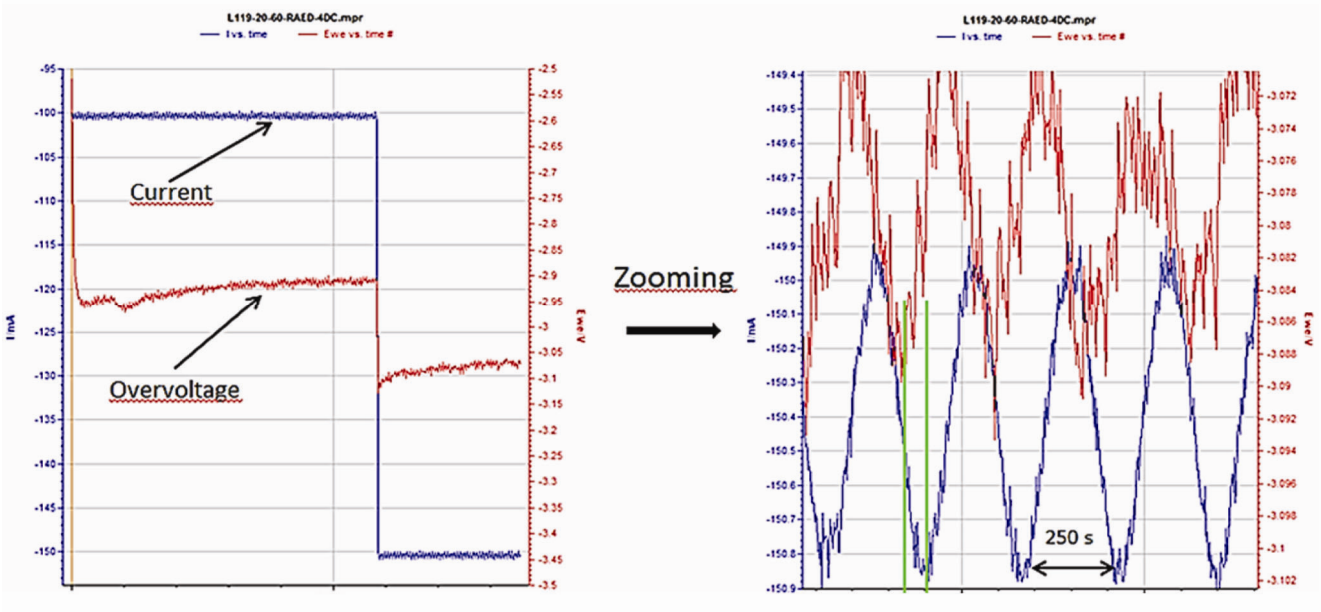

Figure 28. Evidence for oscillating behaviour during excess power production by sample L119(20–60). Both current and over-voltage show a sine-like fluctuation. The amplitudes of the fluctuations are roughly 0.5 mA and 1 mV respectively.

Figure 27 *b*. Evidently, the PSDF is different from that representing the surface status before the electrolysis, as shown in Figure 19 *b*. We observe again a large peak at $k = 1\ \mu m^{-1}$ and other smaller peaks around $k = 2–5\ \mu m^{-1}$. The small plot inside Figure 27 *b* is a zoom of the PSDF concerning a different point on the same surface. It turns out that in this case also the excess is correlated to a sample that has regions on the surface with the same features typically displayed by active electrodes. This paves the way for understanding why, in certain situations, the excess power was produced after a long electrolysis. The explanation could be that the electrochemical process may produce, after some time (necessary not only for loading), the appropriate features required to observe the onset of the effect. It turns out that the different electrochemical interface structure characterizing the active status led one to consider a resonant mechanism linked to the status of the surface that sometimes is created during the electrochemical process.

In order to attempt to explain why the surface morphology was modified during electrolysis. During the excess produced by the sample L119(20–60), as already

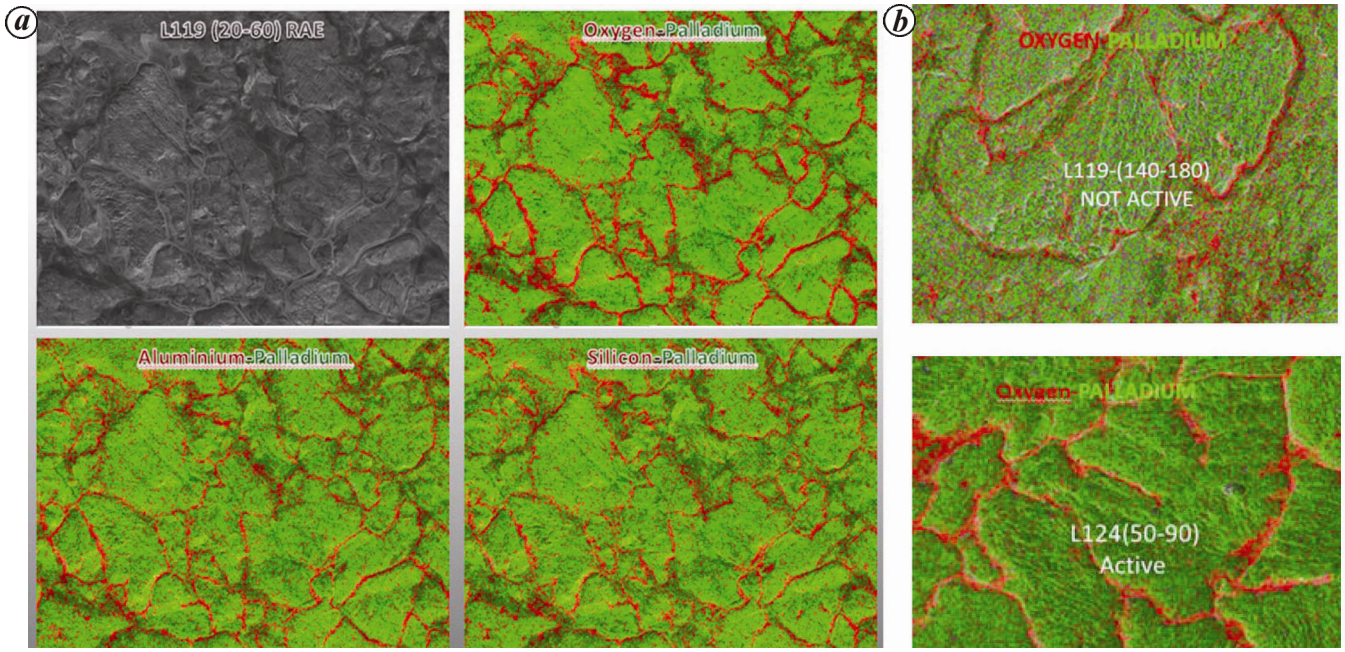

Figure 29. ***a***, Surface analysis of the sample L119(20–60) before electrolysis; the SEM microanalysis reveals the presence of Al and Si oxides impurities mostly placed into the grain boundary. ***b***, Not active sample belonging to lot L119 and active sample L124(50–90).

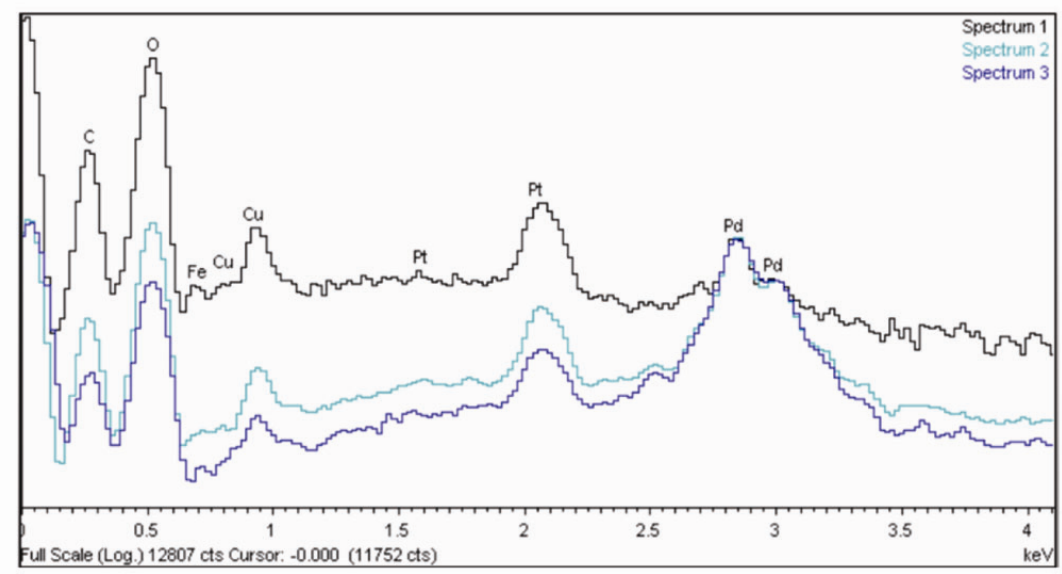

Figure 30. Quantitative spectra, normalized on Pd peak (log scale), performed on the sample L119(20–60) as it was producing excess power.

observed for excesses of significant amplitude, the current showed a ripple that is not expected to exist during galvanostatic operation. Figure 28 (left) shows the current and over-voltage ripples. The over-voltage ripple is typically due to the formation of bubbles, but this signal has a random evolution. Since the ripple on the current was unexpected, we zoomed both the signals (right side of Figure 28). We observed clear current and voltage oscillations, which we may trace back to an electrochemical oscillation (the behaviour is inductive since the current signal is delayed). The effect of electrochemical oscillations as a technique for producing sub-micrometric structures is described in the literature[25,26]. This has no effect on the calorimetric measurement, as explained above, and, in addition, in the present case, the current oscillation has an amplitude of 0.5 mA only.

Electrochemical oscillations that are well known and largely described in the literature are low frequency processes, but the experimental evidence led to investigate the aspect of RF signal emission during excess power. This

study was pioneered by Dominquez *et al.*[27] and continued in order to investigate a large frequency range[28]. The frame emerging from this analysis is pointing in the direction of a significant electrodynamics process existing at the electrode interface during excess power production that seems to be linked to material features and the electrochemical status.

We now comment on some other properties of the cathodes related to the chemical status of the surface before electrolysis and during the event. The study was performed by using SEM micro-analysis technique and surface analysis before electrolysis. The EDX (energy dispersive X-ray analysis) maps reveal Al and Si as contaminants, as oxides, mostly placed into the grain boundary. This presence of oxides on active electrodes has been already reported[17] as an important condition to have better reproducibility with PdRh samples. The effect of these contaminants on the surface is still under study, but is clear that Al and Si are not only contaminants of the raw palladium but are also delivered, sometime, by the crucible during the preparation of PdRh alloy. The oxides EDX map of the sample L119(20–60) is shown in Figure 29 *a*. Other samples have been obtained from the same annealed and rolled $Pd_{90}Rh_{10}$ foil used to prepare the sample L119(20–60), but none of them was active. Four other lots of PdRh alloy have been prepared before obtaining the sample L124(50–90) showing the same features as L119(20–60); moreover, this sample was active and characterized by good loading dynamics.

Figure 29 *b* shows the same map for a inactive electrode belonging to the same L119 lot and for an active sample L124(50–90) from a different lot.

It turns out again that the probability of reproducing the effects lies in the reproducibility of some material features. Figure 30 shows the results of the micro-analysis done on the texture found on the surface of the sample L119(20–60). Most of the cathode is covered by the texture and iron and copper are supposed to come from electric connectors, while platinum is released by the anodes. This layer does not greatly affect the high loading that was maintained during the effect.

Conclusions

This work has highlighted the importance of materials science to achieve all the conditions, i.e. proper surface morphology, alloy composition, contaminant control, grain size and orientation, necessary for observing the onset of excess of power. Materials science allowed us to rebuild active palladium cathodes having features very close to those yielding excess power. The results show that the reproducibility of the effect is linked to the reproducibility of inducing specific properties in the materials. The role of contaminants seems to be crucial to obtain samples with the required characteristics.

The electrochemical impedance spectroscopy, performed *in situ* during excess power production, even if it is to be considered preliminary, reveals the presence of resonant components, inside the equivalent circuit at the surface/electrolyte boundary.

Electrochemical literature[24] describes high characteristic frequency conditions for partially blocked porous electrodes; however, there are several mechanisms, not necessarily purely electrochemical, that could produce high frequency electromagnetic signals at the electrode interfaces. Nevertheless, although high-frequency systems are assumed to exist in electrochemical systems, the literature explicitly mentions that proper instruments to study such specific electrochemical matter do not exist. Material status is a key to observing the effect. Materials science is the key to understanding it, since some material characteristics support a few processes rather than others.

By applying the scientific method, future work should be oriented towards the definition of the effect rather than its demonstration.

Appendix 1

Here, we approach the question of identifying the error in estimating the input power due to a ground loop that allows some current, which is not detected by the measurement chain, to flow through the cell.

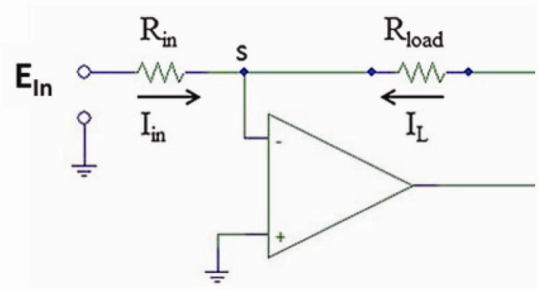

Figure A1. Simplified scheme of a galvanostat.

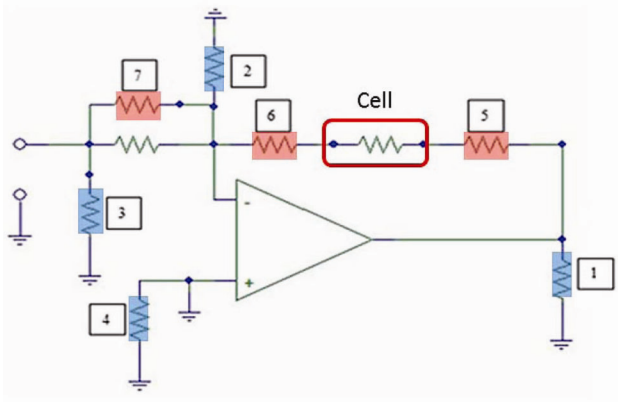

Figure A2. Simplified scheme of a galvanostat with possible connections to ground.

The galvanostat roughly uses the circuit shown in Figure A1 to control the current independent of the load resistance. In the operational amplifier no current is drawn into either the inverting [–] or non-inverting [+] inputs. It serves to keep the potential difference between [+] and [–] inputs zero; hence [–] is at a virtual ground. This point is not connected to ground, but is held at ground potential so the current from the input (control) potential, E_{In}, that flows through the input resistor, R_{In}, is E_{In}/R_{In}. Since no current flows into [–], the current sums at the summing point [*S*] to zero, and $I_{Load} = -E_{In}/R_{In}$, independent of R_{Load}.

The asserted error is a ground loop (or inadvertent low resistance path to ground). Figure A2 shows all possible such pathways (4) in blue with other possible inadvertent or deliberate resistance in red (3).

Let us look at how each of these might affect the control or measurement. First we will look at the 'ground loops' (blue, Figure A2).

(1) A resistance at position [1] from the amplifier output to the ground does nothing. At some point a (real) amplifier may not deliver current or power (or may warm up), but the control loop still functions and the equations above remain exactly the same.

(2) A resistance from the summing point [*S*] to ground does nothing as well. Since this point is held actively at ground potential, no current can flow through resistor [2]. In a real amplifier, this point may vary infinitesimally from virtual ground, especially at high frequencies where the operation amplifier (Op Amp) gain rolls off, but any error will be small.

(3) A resistance to ground across the control voltage source [3] does nothing until the resistance value becomes comparable with the R_{In} voltage supply output resistance. At this point the currents I_{In} and I_{Load} will start to drop, but the load will still be well controlled and constant, and conservative with respect to the command set point.

(4) A resistance [4] to ground from the non-inverting input [+] will not change the outcome of the circuit as the non-inverting input is already tied to ground.

Let us see what other resistors might do (red, Figure A2).

(5) Since the current in the feedback loop is independent of R_{Load}, we can tolerate additional resistance or resistors in that loop and usually place them there deliberately for the reasons clarified in point '7' below, to directly measure the current (rather than relying on E_{In} and R_{In}), Resistor [5] is the 'high side shunt'. It may be as large (up to the voltage compliance of the power supply).

(6) Resistor [6] is the 'low side shunt'. For control purposes it may also be large in combination with [5] up to the voltage compliance of the power supply. Since both are in the control loop, there is no reason for high and low side shunts to report different current values, but the possibility of a new 'ground loop' occurring from the point between R_{Load} and the low side shunt, R6, makes the high side a more conservative place to measure if the shunt has high resistance, and dictates that any shunt on the low side be of small value.

(7) Finally, we come to a place where a resistance leak might make a difference. An inadvertent and unseen resistance shorting R_{In} will cause the current in the load circuit (feedback loop) to be larger than specified or intended. In this (hypothetical) new condition, $I_{In} = E_{In}$ now divided by the parallel combination of R_{In} and R_7…, which will always be greater than intended. Since $I_{Load} = -I_{In}$, the current will control, still well, but at a point higher than that specified by the computer. Hence the need for a shunt to measure independently the current and not simply to assume it is as commanded.

1. Fleishmann, M. and Pons, S., Electrochemically induced nuclear fusion of deuterium. *J. Electroanal. Chem*., 1989, **261**, 301.
2. McKubre, M. C. H., Crouch-Baker, S., Riley, A. M., Smedley, S. I. and Tanzella, F. L., Excess power observation in electrochemical studies of the D/Pd system; the influence of loading. In Proceedings III International Conference on Condensed Matter Nuclear Science, Nagoya, Japan, 20–25 October 1992, p. 5.
3. Kunimatsu, K., Hasegawa, N., Kubota, A., Imai, N., Ishikawa, M., Akita, H. and Tsuchida, Y., Deuterium loading ratio and excess heat generation during electrolysis of heavy water by a palladium cathode in a closed cell using a partially immersed fuel cell anode. In Proceedings III International Conference on Condensed Matter Nuclear Science, Nagoya, Japan, 20–25 October 1992, p. 31.
4. Violante, V. *et al.*, Material science on Pd–D system to study the occurrence of excess of power. In Proceedings XIV International Conference on Condensed Matter Nuclear Science, Washington DC, 10–15 August 2008, vol. 2, pp. 429–436.
5. Violante, V. *et al*., Evolution and progress in material science for studying the Fleischmann and Pons effect (FPE). In Proceedings XV International Conference on Condensed Matter Nuclear Science, Rome, Italy, 5–9 October 2009, p. 1.
6. Violante, V. *et al*., The study of the Fleischmann and Pons effect through the materials science development. In Proceedings of the XVI International Conference on Condensed Matter Nuclear Science, Chennai, India, 6–11 February 2011, p. 313.
7. Violante, V. *et al*., Excess of power during electrochemical loading: materials, electrochemical conditions and techniques. In Proceedings XVIII International Conference on Condensed Matter Nuclear Science, Columbia, MU, USA, 20–25 July 2013.
8. Adrover, A. *et al*., Stress induced diffusion of hydrogen in metallic membranes, cylindrical vs planar formulations I. *J. Alloys Comp. I*, 2003, **358**(1), 268–280.
9. Adrover, A. *et al*., Stress induced diffusion of hydrogen in metallic membranes, cylindrical vs planar formulations II. *J. Alloys Comp. I*, 2003, **358**(1), 157–160.
10. Adrover, A. *et al*., Effects of self-stress on hydrogen diffusion in Pd membranes in the coexistence of α and β phases. *J. Alloys Comp. II*, 2003, **358**(1), 287–297.
11. Violante, V. *et al.*, Consequences of lattice expansive strain gradients on hydrogen loading in palladium. *Phys. Rev. B*, 1997, **56**(5), 2417–2420.

12. Knies, D. L. *et al.*, *In-situ* synchrotron energy-dispersive X-ray diffraction study of thin Pd foils with Pd : D and Pd : H concentrations up to 1 : 1. *J. Appl. Phys*., 2012, **112**, 083510.
13. Memming, R., *Comprehensive Treatise of Electrochemistry*, Plenum Press, New York, 1983, vol. 7.
14. Dardik, L. *et al*., Excess heat in electrolysis experiments at Energetics Technologies. In Proceedings XI International Conference on Cold Fusion, Marseille, France, 31 October–5 November 2004, p. 84.
15. Bertalot, L., De Marco, F., De Ninno, A., La Barbera, A., Scaramuzzi, F., Violante, V. and Zeppa, P., Study of deuterium charging in palladium by electrolysis of heavy water: heat excess production. *J. Nuovo Cimento*, 1993, **15**(11), 1435.
16. McKubre, M., Tanzella, F. and Violante, V., What is needed in LENR/FPE studies? In Proceedings of XVI International Conference on Condensed Matter Nuclear Science, Chennai, India, 6–11 February 2011, p. 1.
17. Dominguez, D. D. *et al.*, Are oxides necessary in Fleischmann–Pons type experiments? In Proceedings XVI International Conference on Condensed Matter Nuclear Science, Chennai, India, 6–11 February 2011, p. 53.
18. Fast, J. D., *Gases in Metals*, Philips Technical Library, Eindhoven, 1976.
19. Shewmon, P. G., *Diffusion in Solids*, McGraw-Hill, New York, 1963.
20. Spitler, M. T., Effect of nanometer-sized surface morphology upon electrochemical kinetics. *Electrochim. Acta*, 2007, **52**, 2294–2301.
21. Gosàlvez, M. A. and Nieminen, R. M., Surface morphology during anisotropic wet chemical etching of crystalline silicon. *New J. Phys*., 2003, **5**, 100.
22. Bianchi, G. and Mazza, F., *Fondamenti di Corrosione dei Metalli* (ed. Tamburini), Milan, 1975.
23. Knies, D. *et al*., Differential thermal analysis calorimeter at the Naval Research Laboratory. In Proceeding ICCF-15, Rome, Italy, 5–9 October 2009, p. 11.
24. Orazem, M. E. and Tribollet, B., *Electrochemical Impedance Spectroscopy*, John Wiley, NJ, 2008, p. 157.
25. Fukami, K. *et al*., General mechanism for the synchronization of electrochemical oscillations and self-organized dendrite electrodeposition of metals with ordered 2D and 3D microstructures. *J. Phys. Chem. C*, 2007, **111**, 1150–1160.
26. Eftekhari, A., *Nanostructured Materials in Electrochemistry*, Wiley-VGH, 2008, ISBN 978-3-527-31876-6.
27. Dominguez, D. *et al*, In 17th Conference on Condensed Matter Nuclear Science, Daejeon, Korea, 12–17 August 2012; http://lenr-canr.org/acrobat/DominguezDanomalousr.pdf
28. Violante, V., Castagna, E., Lecci, S., Pagano, G., Sansovini, M. and Sarto, F., EAI – Energia Ambiente Innovazione is edited by ENEA, Italian National Agency for New Technologies, Energy and Sustainable Economic Development, 2-3/2014, p. 63; DOI: 10.12910/EAI2014-62.
29. Fazle Kibria, A. K. M., Deuterium solubility and electrical resistance of palladium–rhodium alloys. *Int. J. Hydrogen Energy*, 2000, **25**, 997–1003.